IMPLEMENTATION OF THE CARDIOID EQUATORIAL MICROPHONE ARRAY BASED ON OMNIDIRECTIONAL MICROPHONES

Jens Ahrens
Division of Applied Acoustics
Chalmers University of Technology
412 96 Gothenburg, Sweden

Abstract

Cardioid equatorial microphone arrays are baffleless ambisonic capture devices that use outward facing cardioid microphones arranged on a circle. The microphone mounts are straightforward to manufacture, and the compact form factor produces minimal visual disturbance. But low-cost cardioid microphones with low mismatch are not always readily available. We present an implementation that uses pairs of omnidirectional microphones to create virtual cardioid sensors. This solution poses challenges at low frequencies. Our implementation therefore uses omnidirectional sensors at low frequencies and the virtual cardioid sensors at mid- and high frequencies.

Keywords: *ambisonics, binaural audio, spatial audio, spherical harmonics*

1. Introduction

Equatorial microphone arrays (EMAs) were proposed in [1] as an alternative to spherical microphone arrays (SMAs) for obtaining a spherical harmonic (or *ambisonic*) representation of the captured sound field. The original baffled EMA (see Fig. 1 (left)) is essentially an SMA with all microphones confined to the equator. EMAs can obtain an SH representation of Nth order from $2N + 1$ microphones wheres SMAs require at least $(N + 1)^2$ microphones. This advantage of EMAs comes at the price of some limitations in terms of capturing elevation information from the incident sound field as discussed further below.

The mathematical framework that EMAs build on assumes that the EMA is located in the horizontal plane and that the incident sound field is height invariant. A theoretically accurate orthogonal decomposition of the incident sound field can be obtained that can be formulated as an SH decomposition. In other words, standard ambisonic signals can be obtained from EMAs. If the assumption of height invariance of the incident sound field is fulfilled, which is the case, for example, for sounds originating from sources in the horizontal plane, then the obtained ambisonic signals are an accurate representation of the incident sound field. If the incident sound if is not height invariant, then the EMA produces an SH representation of a horizontal projection of the sound field.

If the EMA uses a spherical baffle, then the assumption of height invariance of the incident sound field is not strictly fulfilled over the entire baffle for sound sources that are in the horizontal plane but very close to the array. It was shown in [1] that for a baffled EMA of radius 0.0875 m, the accuracy of the decomposition is only very mildly affected even when the sound source is at a distance of as close as 0.3 m from the array center.

Sound waves that impinge from non-horizontal directions violate the assumption of height invariance clearly. The horizontal projection of this sound field can still be very useful. For example, when perform-

Figure 1: 5th-order EMA with pressure sensors and baffle, $R = 40$ mm (left), and 3rd-order EMA with virtual cardioid sensors and no baffle, $R = 60$ mm (right).

Corresponding author: *jens.ahrens@chalmers.se.*

ing binaural rendering of the obtained SH signals, the spectral balance of the binaural output signal is hardly affected and even interaural time and level differences are correctly maintained even for the non-horizontal sound field components [2].

The baffled EMA from [1] as well as baffled SMAs use pressure, i.e. omnidirectional, microphones. Alternative baffleless designs that employ cardioid sensors were explored in [2] (EMA) and in [3], [4] (SMA). A cardioid EMA exhibits a very convenient form factor in that it is essentially only a ring of microphones. See Fig. 1 (right). Given that suitable cardioid microphones may not always be readily available, we investigate in this paper the baffleless EMA design from Fig. 1 (right) that employs virtual cardioid sensors that are created from pairs of closely spaced omnidirectional microphones.

Creating cardioid microphones from pairs of omnidirectional microphones has been carried out in many locations in the literature. It is a well known concept, for example, in the context of hearing aids. See [5] for an overview. In the context of general purpose audio capture, it was used, for example, in [6]. We revisit the topic here while focussing on the specific requirements of the present context.

2. The Equatorial Microphone Array

We summarize the mathematical formulation of EMAs in this section. Baffled EMAs were originally proposed in [1], the cardioid EMA was proposed in [2]. We refer the reader to these references for further details. MATLAB implementations and audio examples are available at the URL in Footnote †.

The ultimate goal of the EMA approach is to obtain the spherical harmonic (SH) coefficients $\breve{S}_{n,m}(\omega)$ of the captured sound pressure field. The SH coefficients $\breve{S}_{n,m}(\omega)$ are termed *ambisonic signals* when transferred to time domain [7]. The ability of EMAs to produce standard ambisonic signals integrates EMAs well into the established ambisonic ecosystem [7]. See [2] for further details on the nomenclature that we use. For convenience, we will consider binaural decoding of the ambisonic signals as the targeted application case.

The sound field coefficients $\breve{S}_{n,m}(\omega)$ can be computed from the microphone signals $S^{(\mathrm{X})}(\alpha, R, \omega)$ via

$$\breve{S}_{n,m}(\omega) = \frac{N_{n,m}\left(\frac{\pi}{2}\right)}{B_m^{(\mathrm{X})}(R,\omega)} \frac{1}{2\pi} \int_0^{2\pi} S^{(\mathrm{X})}(\alpha, R, \omega)\, C_m(\alpha)\, \mathrm{d}\alpha \ , \quad (1)$$

where (X) can be "(Open)", "(Rigid cyl.)", "(Card.)", or "(Rigid sph.)" according to the baffle and microphone type that are employed. See also Tab. 1.

We define the orthonormal, real-valued circular harmonics (CH) $C_m(\alpha)$ as

$$C_m(\alpha) = \begin{cases} \sqrt{2}\sin\left(|m|\alpha\right), & \forall m < 0 \\ 1 & , \forall m = 0 \\ \sqrt{2}\cos\left(m\alpha\right), & \forall m > 0 \end{cases} . \quad (2)$$

To avoid confusion with the order n in SH decompositions, we refer to m as the *degree*.

$$N_{n,m}(\beta) = (-1)^m \sqrt{\frac{2n{+}1}{4\pi}\frac{(n{-}|m|)!}{(n{+}|m|)!}}\, P_n^{|m|}(\cos\beta) \ , \quad (3)$$

whereby $P_n^m(\cdot)$ are the associated Legendre functions. Eq. (1) requires that the microphones are continuously distributed along the circular microphone contour. In practice, the integral along the microphone contour has to be replaced with a summation over the signals from the discrete microphones, which produces spatial aliasing at high frequencies.
The radial terms $B_m(R,\omega)$ become very small at low frequencies and high degrees $|m|$ so that the inverse of $B_m(R,\omega)$ in (1)* – the *radial filters* – needs to be regularized, for example, using Tikhonov regularization [8]. This is an aperture effect and represents the fact that it requires aggressive processing to extract detailed spatial information from the captured sound field at low frequencies where the wavelength is much longer than the dimensions of the array. This is a general challenge for all compact spatial microphone array designs incl. SMAs, and the quantitative difference between different array designs is very small [9], [10]. As discussed in [11], this is not necessarily a limitation when binaural rendering of the captured sound field is targeted as only certain spatial information is required for computing the binaural output signals in this case.

Baffle / sensor type	Identifier	$B_m(R,\omega)$
No baffle / pressure	(Open)	$\mathrm{i}^m\, J_m\left(\omega\,\frac{R}{c}\right)$
Rigid cylinder / pressure	(Rigid cyl.)	$\mathrm{i}^m\, \frac{2}{\pi\mathrm{i}\omega\,\frac{R}{c}}\, \frac{1}{H_m'\left(\omega\,\frac{R}{c}\right)}$
No baffle / cardioid	(Card.)	$\mathrm{i}^m\, \left[J_m\left(\omega\,\frac{R}{c}\right) - \mathrm{i}J_m'\left(\omega\,\frac{R}{c}\right)\right]$
Rigid sphere / pressure	(Rigid sph.)	$\sum_{n'=\lvert m\rvert}^{\infty} b_{n'}(R,\omega)\, \left[N_{n',m}(\pi/2)\right]^2$

Table 1: $B_m(\omega, R)$ for the most common types of setups. The cardioid microphones point radially outwards. $J_m(\cdot)$ is the Bessel function of order m, $H_m(\cdot)$ is the mth-order Hankel function of second kind, and the prime $'$ denotes the derivative with respect to the argument. $N_{n,m}(\cdot)$ is defined in (3) and $b_n(\cdot)$ in [2, Eq. (4)].

3. The Radial Filters

Fig. 2 (left) depicts the magnitudes of the component $1/B_m^{(\mathrm{Card.})}(R,\omega)$ of the unregularized inverse radial terms of the cardioid EMA. (The term $N_{n,m}\left(\frac{\pi}{2}\right)$ applies an additional frequency independent scaling.)

*For convenience, we define the radial filters as $N_{n,m}\left(\frac{\pi}{2}\right)/B_m^{(\mathrm{X})}(R,\omega)$, see (1), which is the equivalent to the established SMA radial filters.

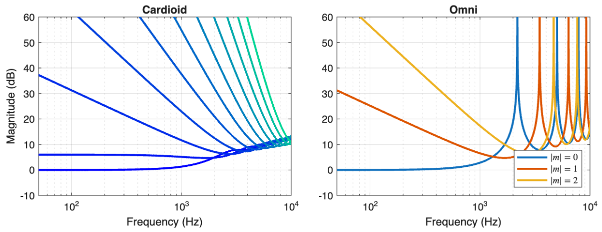

Figure 2: Magnitude of the unregularized terms $1/B_m^{(\mathrm{Card.})}(R,\omega)$ for degrees $|m| = 0..7$ (from blue to green, left plot) and $1/B_m^{(\mathrm{Omni})}(R,\omega)$ for degrees $|m| = 0, 1, 2$ (right plot). $R = 0.06$ m.

Recall from Footnote * that these are directly proportional to what we define as radial filters. See [2] for a discussion of the complete EMA radial filters as defined in Footnote *. We do not summarize this discussion here as it appears to be an unnecessary distraction.

We will demonstrate in Sec. 4 and 6 that the implementation of virtual cardioid microphones via pairs of omnis causes difficulties at very low frequencies. Fig. 2 (right) shows that the singularities of the terms $1/B_m^{(\mathrm{Omni})}(R,\omega)$ of a baffleless EMA with omnidirectional (pressure) microphones occur only above a certain frequency and that this frequency increases with increasing degree $|m|$. For the assumed nominal array radius of $R = 0.06\,\mathrm{m}$ of our prototype, singularities occur only around $2\,\mathrm{kHz}$ and higher. We will therefore implement the proposed EMA in a hybrid fashion that will use a single ring of omnidirectional microphones up to a frequency of f_c where this omni solution is more robust and more straightforward to implement. We mention this here because this choice facilitates the creation of virtual cardioid microphones from pairs of omnis as presented in Sec. 4.

4. Creating Virtual Cardioid Sensors From Pairs of Omnis

We do not have cardioid microphones with a suitable form factor and small enough mismatch available. We therefore implemented the cardioid EMA prototype using pairs of closely-spaced omnidirectional microphones as depicted in Fig. 1 (right) whereby each pair of omnidirectional microphones is converted into a radially outward facing virtual cardioid microphone. In the remainder, we will assume the geometry depicted in Fig. 3.

The signal $S_{\mathrm{card.}}(\vec{\mathbf{x}}_0,\omega)$ from a cardioid sensor at $\vec{\mathbf{x}}_0$ pointing in direction of the unit-length vector $\vec{u}$ can be described as [10]

$$S_{\mathrm{card.}}(\vec{\mathbf{x}}_0,\omega) = S(\vec{\mathbf{x}}_0,\omega) + \frac{1}{\mathrm{i}\frac{\omega}{c}}\,\vec{u}^T\,\nabla S(\vec{\mathbf{x}},\omega)\Big|_{\vec{\mathbf{x}}=\vec{\mathbf{x}}_0} . \quad (4)$$

$S(\vec{\mathbf{x}}_0,\omega)$ is the sound pressure at $\vec{\mathbf{x}}_0$. ($S(\vec{\mathbf{x}}_0,\omega)$ can be approximated by the signal of either of the two microphones in the pair. We have not observed that it makes a noteworthy difference which one is being used.) Note that (4) produces a cardioid with sensitivity 2 in on-axis direction. We will assume in the remainder that $S(\vec{\mathbf{x}}_0,\omega)$ is normalized by 0.5 to produce unit sensitivity on-axis.

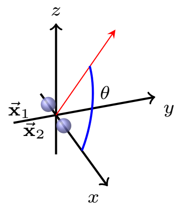

Figure 3: Local coordinate system with its origin at the nominal location $\vec{\mathbf{x}}_0$ of the virtual cardioid sensor. The positive x-direction is on-axis, and θ is the angle between the sound incidence direction, which is indicated by the red arrow, and on-axis. In the prototype from Fig. 1 (right), the microphones are located at $\vec{\mathbf{x}}_{2,1} = [\pm 3.5\,\mathrm{mm}, 0, 0]^T$.

The sound pressure gradient $\nabla S(\vec{\mathbf{x}},\omega)$ can be approximated from the two omni-signals via the corresponding difference quotient as

$$\nabla S(\vec{\mathbf{x}}_0,\omega)\Big|_{\vec{\mathbf{x}}=\vec{\mathbf{x}}_0} \approx \frac{S(\vec{\mathbf{x}}_2,\omega) - S(\vec{\mathbf{x}}_1,\omega)}{\|\vec{\mathbf{x}}_2 - \vec{\mathbf{x}}_1\|} . \quad (5)$$

$\vec{\mathbf{x}}_0$ is the midpoint between $\vec{\mathbf{x}}_1$ and $\vec{\mathbf{x}}_2$. The difference quotient cannot be regarded as an approximation of the gradient at frequencies where $\|\vec{\mathbf{x}}_2 - \vec{\mathbf{x}}_1\|$ is larger than half the wavelength because spatial aliasing arises. Our prototype from Fig. 1 (right) uses a spacing of $7\,\mathrm{mm}$, which corresponds to the half wavelength at approx. $16\,\mathrm{kHz}$.

Simulating (4) in frequency domain is straightforward apart from DC where it is undefined. Obtaining a time domain representation of (4) by Fourier transforming the frequency domain representation with regularized DC is not practical. We therefore seek a solution via filter design.

We will argue in the following sections that it will be favorable to implement the EMA using a hybrid solution that uses the virtual cardioids as described above only above a frequency f_c and the "(Open)" configuration (Tab. 1) below f_c. This provides us with some freedom to deviate from the exact implementation of (4) at low frequencies.

The term $^1/_{\mathrm{i}\omega}$ in (4) is an integrator, which is undefined at DC. A practical solution for creating virtual cardioid microphones needs to counteract the $^1/_\omega$ slope of the integrator at low frequencies to achieve finite amplification at DC. Similar to [6], [12], we choose to make the integrator leaky by adding a Butterworth highpass filter that we obtain through a bilinear transform of the time-continuous representation. A first-order highpass filter has a slope proportional to ω below the cuttoff and ensures a constant (but high) amplification at DC. Higher-order highpass filters force the amplification at DC to zero, which may appear preferable. However, Fig. 4 shows that the phase response of highpassed integrators deviates stronger from the target response in the passband of the high-

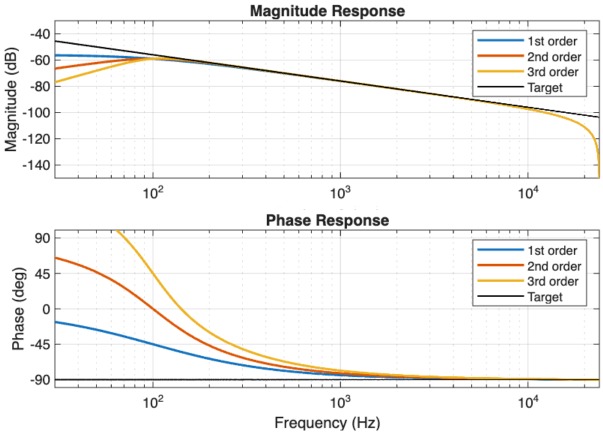

Figure 4: Simulated magnitude and phase response of digital highpassed integrators for different orders of the Butterworth highpass filters. The black lines represent the target response $^1/_{i\omega}$. The cutoff frequency f_{hp} of the highpasses is 100 Hz.

pass filters. When using these highpassed integrators to create virtual cardioid microphones according to (4), it turns out that the polar patterns of the resulting virtual cardioid sensors as well as their angle dependent transfer functions deviate stronger from the desired ones as illustrated in Fig. 5 and 6.

The transition to omnidirectional directivity at low and high frequencies (and the associated msgnitude drop from 0 dB to -6 dB for the on-axis direction), where the highpassed digital integrator's magnitude response attenuates the gradient component of the directivity, is particularly strongly apparent in Fig. 5. Fig. 5 shows, too, that the deviations of the phase response of the highpassed integrator are detrimental to the directivity and magnitude response of the resulting virtual cardioid sensors. We will therefore use the 1st-order highpass in the remainder.

Fig. 7 depicts the measured polar patterns of one of the virtual cardioids in the prototype from Fig. 1 (right) that was obtained using a highpassed integrator as described above with $f_{\mathrm{hp}} = 10$ Hz (We used $f_{\mathrm{hp}} = 100$ Hz in Fig. 4-6 for illustration purposes. We use $f_{\mathrm{hp}} = 10$ Hz for the actual implementation). It can be seen that the directivity is indeed cardioid for the vast part of the frequency range. Small deviations arise at $f = 6.4$ kHz and moderate ones at $f = 12.8$ kHz. Note that this is a frequency range where spatial aliasing is apparent if the array is used for sound field capture so that the deviations of the directivity from cardioid may be tolerable at such high frequencies. The measurement data for $f = 100$ Hz are noisy because of the reasons explained in Sec. 6.

5. The Hybrid Solution

Because of the limitations of the implementation of the integrator in (4) discussed in the previous section, we avoid using the signals from the virtual cardioid sensors at frequencies below $f_c = 800$ Hz where we use the array in the `Omni` configuration (recall Tab. 1),

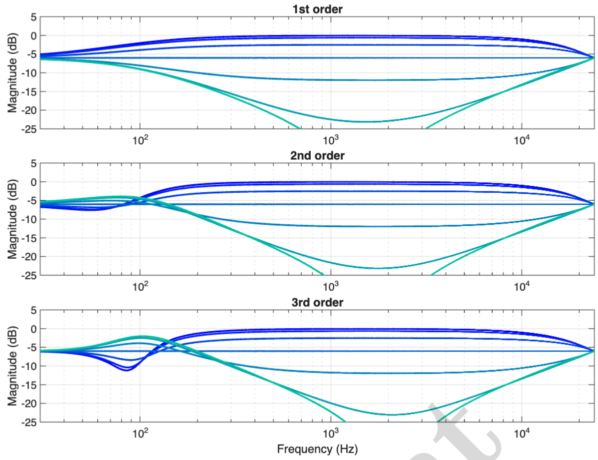

Figure 5: Simulated magnitude transfer functions of virtual cardioids for plane wave incidence from the angles from 0° to 180° in steps of 45° (blue to green) relative to on-axis. $f_{\mathrm{hp}} = 100$ Hz for different orders of the highpass. The spacing between the omnis is 7 mm.

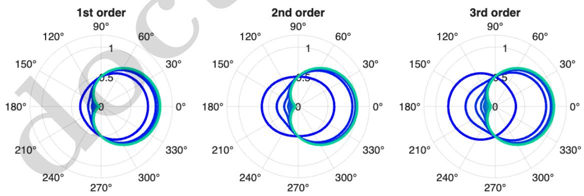

Figure 6: Simulated polar patterns for the virtual cardioids from Fig. 5 for frequencies between 100 Hz and 1000 Hz in steps of 100 Hz (blue to green).

i.e. we use a single ring of omnidirectional microphones in this frequency range. As it will become evident in Sec. 6, it is favorable to select f_c to be as high as possible. We choose $f_c = 800$ Hz, which avoids that the output signals are affected by the singularity of $1/B_m^{(\mathrm{Omni})}(R, \omega)$ at $m = 0$ (recall Fig. 2 (right)). We use a Linkwitz-Riley crossover between the two frequency ranges.

Fig. 8 shows depicts binaurally decoded signals simulated using the parameters of the prototype from Fig. 1 (right), i.e. a nominal radius of 60 mm, a spacing of 7 mm between the microphones in each of the 7 pairs. The array produces a 3rd-order ambisonic signal. We used the head-related transfer functions (HRTFs) of a rigid spherical head with no pinnae for convenience.

It can be seen that the binaural signals are exact below 1 kHz. The hump around 2 kHz and the too low magnitude above 5 kHz are a consequence of the order limitation and occur with any type of array [11]. Spatial aliasing is apparent above 5 kHz, too, whereby the cardioid EMA from omnis shows some more additional artifacts, which are most likely due to the fact that the virtual cardioid signals are less exact

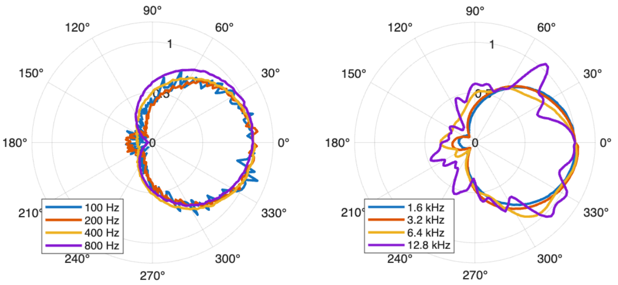

Figure 7: Measured directivity of one of the virtual cardioids in the prototype from Fig. 1 (right) normalized to 0° (on-axis). The spacing between the microphones is 7 mm.

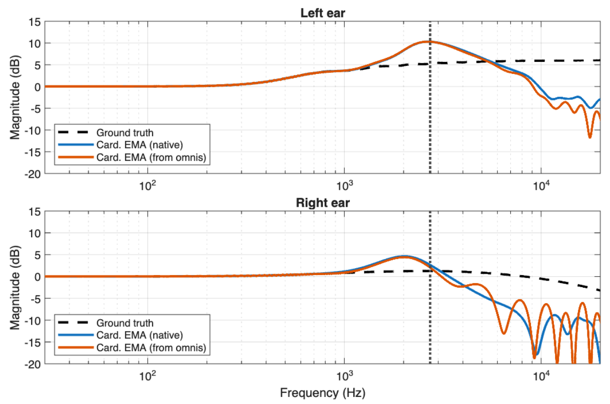

Figure 8: Simulated binaural signals from the 3rd-order prototype array from Fig. 1 (right) for sound incididence from $90^\circ$to the left and when using rigid-sphere HRTFs. The data for `Card. EMA (native)` were computed in frequency domain. The data for `Card. EMA (from omnis)` were computed in time domain. The black dotted vertical line is the frequency at which $kR = N$.

in this frequency range. Given that the additional artifacts due to the virtual cardioid microphones occur only where there is spatial aliasing, too, these artifacts appear to be tolerable (see the audio examples linked in Footnote †). It is also worth highlighting that the non-ideal properties of the digital highpassed integrator do not appear to affect the binaural signals to a noteworthy extent. We refer the reader to [2] for more binaural signals obtained from the native cardioid EMA.

6. Microphone Self-Noise

Eq. (4) and (5) deserve a closer look into their properties regarding how they handle microphone self noise. Whenever a signal processing operation combines two or more signals by multiplying the signals with a number that is large compared to the overall gain of the operation, independent noise in the signals is amplified. When creating a virtual cariodid from a pair of omnis, division by small numbers occurs in the factor $\frac{1}{\mathrm{i}\frac{\omega}{c}} = \frac{1}{\mathrm{i}k}$ in (4) and in the difference quotient in (5). $k = 2\pi f/c = 1/\mathrm{rad}$ at a frequency of approximately 55 Hz and accordingly smaller at lower frequencies. It is desirable to use a small spacing $\|\vec{\mathbf{x}}_2 - \vec{\mathbf{x}}_1\|$ between the microphones in a pair to make the difference quotient approximate the gradient as best as possible. The large amplification of self noise by the virtual cardioid sensor is well known in context of hearing aids [5].

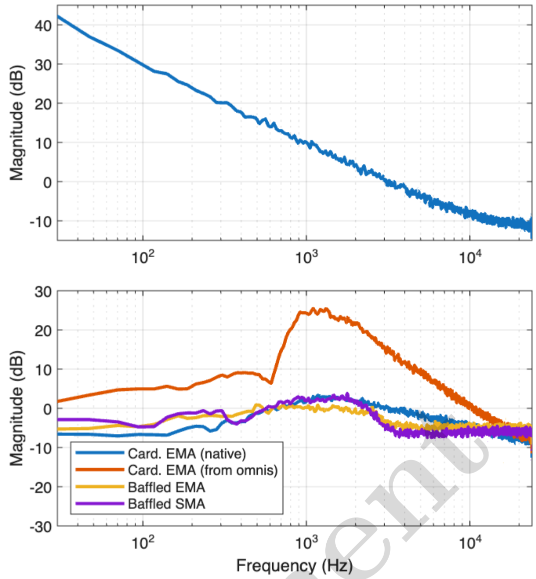

Figure 9: Top: Estimate of the PSD of a single virtual cardioid with a spacing of 7 mm between the omnis. Bottom: Estimate of the PSD of microphone noise in the binaural output of the prototype from Fig. 1 (right). The PSD at each microphone is 1. `Card. EMA (native)` is an EMA with actual cardioid sensors. `Card. EMA (from omnis)` is the proposed hybrid solution. The transition between omni and virtual cardioid is at 800 Hz. `Baffled EMA` is the one presented in [1]. For comparison, the data for a 3rd-order baffled SMA with 25 microphones on a Fliege grid are also depicted. $f_{\mathrm{hp}} = 10$ Hz in all cases.

Fig. 9 (top) depicts the power spectral density (PSD) of the microphone self noise at the output of a single virtual cardioid microphone if each microphone in the pair exhibits self noise with a PSD of 0 dB. Positive figures mean that the signal processing amplifies self noise compared to the target signal, negative figures mean that the signal processing attenuates self noise. It is approximately at 3 kHz that the factors $1/k$ and $1/\|\vec{\mathbf{x}}_2 - \vec{\mathbf{x}}_1\|$ cancel each other out so that the noise PSD at the output is exactly 0 dB.

As a consequence of the virtual cardioid amplifying self noise to a considerable extent, a cardioid EMA that is composed of virtual cardioids amplifies self noise accordingly as illustrated in Fig. 9 (bottom). The signal processing pipeline was calibrated such that the root mean square (RMS) of the target signal in the binaural output corresponds to the RMS of the target signal in the signal of the microphone that faces in the directiom from which that target signal impinges.

It can be seen in Fig. 9 (bottom) that EMAs and SMAs exhibit comparable properties with respect to self noise apart from `Card. EMA (from omnis)` in that they increase the signal to noise ratio slightly [13]. The change of noise level around f_c for the `Card. EMA (from omnis)` is clearly apparent in Fig. 9 (bottom). The high noise amplification of the virtual cardioid sensors is a concern in practice. See Sec. 7 for mitigation measures and other comments on our prototype. The singularities of the radial filters of the `Open` configuration occur at higher frequencies, with higher degrees $|m|$ being considered (recall Fig. 2 (right)). It may be possible to reduce the noise in the output signals by some amount by using a degree dependent crossover between `Open` and `Virtual Card.` that uses the `Open` configuration up to higher frequencies at higher degrees $|m|$. We have not explored this option.

7. Further Comments on the Implementation

We provide a demonstration video of our 14-microphone, 3rd-order prototype from Fig. 1 (right) and MATLAB code for the signal processing at†. We found that the high noise gain is indeed a concern in practice. The video demonstrates the use of a multichannel Wiener filter for suppressing noise in the array signals before the array processing. The filter operates in the short-time Fourier transform domain and uses a covariance matrix of the self noise that is obtained from a short recording (i.e., a second or so) of the self noise. The video shows that such a filter can indeed be very effective.

Just like SMAs, it is very beneficial if the microphones are calibrated with respect to their sensitivity. We calibrated our microphones based on measurements that we conducted in an anechoic chamber. We calibrated the sensitivity in a frequency independent manner based on the root mean square of the measured signals in the frequency range between 100 Hz and 800 Hz. The sensitivity differences in the given frequency range were up to ±1.5 dB before calibration. The Røde Lavalier GO microphones that we used exhibit a noteworthy frequency dependent mismatch of up to several dB even after calibration of the sensitivity. It seems that this mismatch is tolerable in practice although we have not investigated this matter in detail.

8. Conclusions

It is feasible to create a cardioid equatorial microphone array based on pairs of omnidirectional microphones. The virtual cardioid sensors that are created exhibit the desired directivity over the best part of the frequency range of interest.

A noteworthy limitation is the high noise gain that virtual cardioid sensors exhibit. This can be mitigated considerably by state of the art noise suppression as provided, for example, by a multichannel Wiener filter. Future work includes sourcing suitable cardioid sensors with a low enough mismatch. This provides the potential for significantly reducing noise in the array output signals compared to the presented solution.

† `https://github.com/AppliedAcousticsChalmers/ambisonic-encoding`.

References

[1] J. Ahrens, H. Helmholz, D. L. Alon, and S. V. Amengual Garí', "Spherical harmonic decomposition of a sound field based on observations along the equator of a rigid spherical scatterer," *JASA*, vol. 150, no. 2, pp. 805–815, Aug. 2021.

[2] J. Ahrens, "A baffleless equatorial ambisonic microphone array of arbitrary order," in *AES Conf. on AVARIG*, Paris, France, Jun. 2026.

[3] F. Melchior, O. Thiergart, G. D. Galdo, D. de Vries, and S. Brix, "Dual radius spherical cardioid microphone arrays for binaural auralization," in *127th Conv. of the AES*, 2009.

[4] M. R. P. Thomas, "Practical concentric open sphere cardioid microphone array design for higher order sound field capture," in *IEEE International Conference on Acoustics, Speech and Signal Processing (ICASSP)*, 2019, pp. 666–670.

[5] T. A. Ricketts, "Directional hearing aids," *Trends in Amplification*, vol. 5, no. 4, pp. 139–176, 2001.

[6] T. Deppisch and C. Frank, "Recording first-order ambisonics with a differential array of two dual-diaphragm microphones," in *148th Conv. of the AES*, 2020.

[7] F. Zotter and M. Frank, *Ambisonics: A Practical 3D Audio Theory for Recording, Studio Production, Sound Reinforcement, and Virtual Reality.* Heidelberg: Springer, 2019, Freely available at `https://link.springer.com/book/10.1007/978-3-030-17207-7`.

[8] S. Moreau, J. Daniel, and S. Bertet, "3D sound field recording with higher order ambisonics–objective measurements and validation of a 4th order spherical microphone," in *120th Convention of the AES*, 2006, pp. 20–23.

[9] H. Teutsch, *Modal Array Signal Processing: Principles and Applications of Acoustic Wavefield Decomposition.* Springer, 2007.

[10] I. Balmages and B. Rafaely, "Open-sphere designs for spherical microphone arrays," *IEEE Transactions on Audio, Speech, and Language Processing*, vol. 15, no. 2, pp. 727–732, 2007.

[11] J. Ahrens, "How small can a baffled ambisonic microphone array be?" In *Proc. of DAGA*, Hannver, Germany, Mar. 2024.

[12] I. Henderson, A. Politis, and S. Bilbao, "Filter design for real-time ambisonics encoding during wave-based acoustic simulations," in *Forum Acusticum*, 2020.

[13] H. Helmholz, D. L. Alon, S. V. A. Garí, and J. Ahrens, "Instrumental evaluation of sensor self-noise in binaural rendering of spherical microphone array signals," in *Forum Acu.*, 2020.